MESSENGER Observations of Large Flux Transfer Events at Mercury

James A. Slavin[1], Ronald P. Lepping[1], Chin-Chun Wu[2], Brian J. Anderson[3], Daniel N. Baker[4], Mehdi Benna[5], Scott A. Boardsen[1], Rosemary M. Killen[5], Haje Korth[3], Stamatios M. Krimigis[3,6], William E. McClintock[4], Ralph L. McNutt, Jr[3], Menelaos Sarantos[1], David Schriver[7], Sean C. Solomon[8], Pavel Trávníček[9], and Thomas H. Zurbuchen[10]

Abstract.

Six flux transfer events (FTEs) were encountered during MESSENGER's first two flybys of Mercury (M1 and M2). For M1 the interplanetary magnetic field (IMF) was predominantly northward and four FTEs with durations of 1 to 6 s were observed in the magnetosheath following southward IMF turnings. The IMF was steadily southward during M2, and an FTE 4 s in duration was observed just inside the dawn magnetopause followed ~ 32 s later by a 7 s FTE in the magnetosheath. Flux rope models were fit to the magnetic field data to determine FTE dimensions and flux content. The largest FTE observed by MESSENGER had a diameter of ~ 1 R_M (where R_M is Mercury's radius), and its open magnetic field increased the fraction of the surface exposed to the solar wind by 10 - 20 percent and contributed up to ~ 30 kV to the cross-magnetospheric electric potential.

1. Introduction

The MErcury Surface, Space ENvironment, GEochemistry, and Ranging (MESSENGER) flyby measurements show that Mercury's magnetic field is largely dipolar, has a moment closely aligned with the planet's rotation axis with the same polarity as at Earth, and has not significantly changed since its discovery by Mariner 10 in 1974 and 1975 [*Anderson et al.*, 2008, 2009; *Alexeev et al.*, 2009]. The interaction of the planetary magnetic field with the solar wind is governed primarily by the interplanetary magnetic field (IMF) orientation. For the first MESSENGER Mercury flyby (M1) on14 January 2008 the average IMF upstream of the outbound bow shock was northward with (B_X, B_Y, B_Z) = (-12.9, 4.71, 10.29 nT) in Mercury solar orbital (MSO). In these coordinates X_{MSO} is directed from the center of the planet toward the Sun, Z_{MSO} is normal to Mercury's orbital plane and positive toward the north celestial pole, and Y_{MSO} completes this right-handed orthogonal system. In contrast, for MESSENGER's second Mercury flyby (M2) on 6 October 2008, the mean upstream IMF was southward, (B_X, B_Y, B_Z) = (-15.21, 8.40, -8.51 nT).

Magnetic reconnection occurs at the dayside magnetopause when there is a component of the IMF anti-parallel to the subsolar magnetospheric magnetic field. When such reconnection is localized or non-steady at Earth, discrete magnetic flux tubes with diameters of ~ 1 R_E (1 R_E = 6400 km), termed flux transfer events (FTEs), become connected to the IMF and pulled from the dayside magnetosphere by the anti-sunward flow in the magnetosheath and added to the tail [*Russell and Elphic,* 1978]. FTEs created by reconnection occurring simultaneously at multiple dayside X-lines are identified by their flux rope structure [*Le and Fu, 1985*]. FTEs not possessing flux rope topology may be produced by short duration pulses of reconnection [*Southwood et al.,*

47 1988; *Scholer et al.,* 1988]. They are identified primarily by the characteristic manner
48 in which magnetosheath and magnetospheric magnetic fields drape about these flux
49 tubes as they move tailward.

50 Some FTEs were found and analyzed in the Mariner 10 flyby observations [*Russell*
51 *and Walker*, 1985], and initial examinations of the MESSENGER magnetic field
52 measurements also noted the presence of FTEs [*Slavin et al.,* 2008; 2009a]. Here we
53 report a comprehensive survey of the MESSENGER magnetic field data for the
54 occurrence of FTEs. From definitions developed for Earth's magnetosphere [e.g.,
55 *Wang et al.,* 2005], six FTEs were identified during the two flybys with all, save one,
56 strongly resembling flux ropes. Unfortunately, MESSENER does not make the high
57 time resolution plasma moment measurements necessary to analyze these FTEs using
58 the Grad-Shafranov reconstruction technique [*Zhang et al., 2008; Eriksson et al.,*
59 *2009*]. However, we use a well validated flux rope model [*Lepping et al.*, 1990, 2006]
60 to infer their dimensions, orientation, the proximity of the spacecraft path to the rope's
61 central axis, and their axial magnetic flux content. In contrast with the Mariner 10
62 findings, the MESSENGER results indicate that some FTEs at Mercury carry as much
63 flux as typical FTEs at Earth. It is concluded that these large FTE's will have
64 significant impacts on the cross-magnetospheric electric potential drop and the flux of
65 solar wind ions reaching the surface and sputtering neutrals into Mercury's exosphere.
66

67 **2. MESSENGER Flux Transfer Events Observations**

68 Near the magnetopause, FTEs are identified by variations of the magnetic field in a
69 local boundary-normal coordinate system [*Russell and Elphic,* 1978]. We present data

70 in L-M-N coordinates, where B_N is directed radially outward normal (based upon the
71 *Slavin et al.* [2009a] model) to the closest point on the magnetopause, B_L is
72 perpendicular to B_N and anti-parallel to the planetary magnetic dipole, and B_M
73 completes the right-handed system.

74 We identify two M2 FTE bipolar B_N signatures in Figure 1, the first lasting 3.5 s at
75 08:48:58 UTC and the second lasting 7.1 s at 08:49:30. The sense of the bipolar B_N
76 variation for both FTEs is consistent with reconnection occurring at a tilted X-line
77 passing near the subsolar point and moving northward over MESSENGER. The
78 decrease in magnetic field intensity within the 08:48:58 event is very similar to "crater-
79 type" FTEs at Earth. The crater feature is thought to correspond to a "swirl" of plasma
80 with a high ratio of magnetic to kinetic pressure caused by ongoing reconnection [*Owen*
81 *et al.,* 2008]. The second event at 08:49:30 is the longest duration FTE found in the M1
82 and M2 data and exhibits a strong core magnetic field and helical topology, evident in
83 B_L and B_M, typical of a quasi-force-free flux rope. In this event the core magnetic field
84 exceeds the surrounding magnetosheath field by a factor of ~ 2.5 .

85 Another long-duration FTE lasting 6 s was observed during M1 inbound near the
86 dusk flank. Figure 2 shows data both for this event on the left and for the 7-s FTE
87 discussed above on the right, here presented in MSO coordinates. Vertical dashed lines
88 mark the beginning and end points of each event estimated from the field rotational
89 signature. In each case the flux-rope-like variation in the magnetic field is evident in the
90 rotational signature surrounding an enhancement in the total field. The magnetic field
91 magnitude and rotation in Figure 2a are nearly symmetric relative to the time of
92 maximum field intensity, whereas the FTE in Figure 2b has a narrow, somewhat

93 asymmetric field magnitude enhancement relative to the field rotation. Both of the
94 FTEs are associated with an IMF $B_Z < 0$ in the magnetosheath, as occurred
95 intermittently inbound for M1, but nearly continuously inbound and outbound for M2.
96 Our examination of the MESSENGER magnetic field data revealed three additional
97 magnetosheath FTEs during M1, which are displayed in Figure 3. These FTEs were
98 also associated with magnetosheath $B_Z < 0$ although there is brief (less than 1 min)
99 period of northward magnetic field separating the FTE in Figure 3c from the end of the
100 earlier interval of southward IMF. These FTEs were shorter, lasting ~1 s to 3 s, but they
101 all have magnetic field perturbations similar to the longer-duration events.
102
103 **3. Force-Free Modeling of Flux Transfer Events**
104 We investigate the structure of the FTEs observed by MESSNEGER in Mercury's
105 magnetosheath by modeling them as force-free flux ropes [*Lepping et al.*, 1990].
106 Originally developed for interplanetary magnetic clouds, this procedure has also been
107 applied to a variety of flux ropes in Earth's magnetotail. The model is based on the
108 assumption that the flux rope current density (**J**) and magnetic field (**B**) are related by a
109 constant of proportionality, α;
110 $$\mathbf{J} = \alpha \mathbf{B} \quad (1)$$
111 The structure is assumed to be cylindrically symmetric, with the pitch angle of the
112 helical field lines increasing with distance from the axis of the rope. The field at the
113 center of the rope is aligned with its central axis, becoming perpendicular at the outer
114 boundary of the rope. An analytical approximation for this field configuration is the
115 static, constant-α, force-free, cylindrically symmetric configuration, a solution to

$$\nabla^2 \mathbf{B} = -\alpha^2 \mathbf{B} \quad (2)$$

The *Lundquist* [1950] Bessel function solution is:

$$B_z(r) = B_0 J_0(\alpha r), \quad B_\phi(r) = B_0 H J_1(\alpha r), \text{ and } B_r = 0 \quad (3)$$

where B_0 is the peak axial field intensity and $H = \pm 1$ is the rope's handedness.

Using the method of *Lepping et al.* [1990, 2006], we fit Eq. (3) to the measured magnetic field (in MSO coordinates) for all of the flux rope events.The data are first normalized, and then a variance analysis is applied to establish an approximate rope coordinate system. We then perform a least-squares fit between the normalized, observed magnetic field after transformation into this initial coordinate system, and Eq. (3). Given the orientation of the flux rope relative to the spacecraft trajectory, the radius of the flux rope is inferred from the estimated magnetosheath plasma flow speed. A flow speed of 250 km/s was assumed for the one near-magnetopause FTE and 400 km/s for the other FTEs, on the basis of numerical simulations of solar wind flow about Mercury's magnetosphere for the flybys [*Benna at al.*, 2009; *Trávníčiek et al.,* 2009].

Several parameters were calculated for each flux-rope fit. A "reduced chi" quality parameter, $Q_\chi = \chi/(3N - n)$, was used to measure the quality of the fit, where χ is the variance of the data relative to the fit, N is the number of points considered in the analysis interval, and $n = 5$ is the number of parameters used in the fit. Note that Q_χ is dimensionless since the magnetic field was normalized. A reduced Q_χ of less than 0.25 is required before a fit is regarded as "acceptable" [see *Lepping et al.,* 2006]. The quality of the fit is also judged by the symmetry of the fitted field intensity. We define an asymmetry factor, ASF = $|(1 - 2(t_0/\Delta t)/(N\text{-}1))|$, where t_0 is the center time of the rope and Δt is the sampling interval. An ASF of 0 is an ideal fit to a force-free cylindrical

139 flux rope, and values over 0.5 are not acceptable. Ideally the field is purely azimuthal
140 (i.e., where $\alpha r = 2.4$) at the flux rope boundary, but in practice the precise end-points
141 are not always evident in the data. For this reason trial-fits are generally necessary, with
142 the best fit chosen on the basis of Q_χ and ASF. The flux rope parameters derived from
143 the fits are B_0, the axial field intensity; H, the handedness (+/-1 for right/left hand); R_0,
144 the radius of the flux rope; Y_0, the closest approach distance of the spacecraft to the
145 rope's axis; Y_0/R_0, the "impact parameter;" θ_A and ϕ_A, the polar and longitude angles of
146 the rope's axis, respectively; and t_0, the rope center time.

147 The model fit to the M1 FTE observed at 18:36:20 is displayed in Figure 2a. The
148 best-fit model parameters are given in Table 1 (i.e. Event 3). The agreement between
149 the data and the flux rope model is excellent. The Q_χ and ASF parameters are small,
150 0.082 and 0.20, respectively. The inferred flux rope radius is 0.52 R_M (where R_M is
151 Mercury's radius), and B_0 is 39 nT. The spacecraft closest approach distance was
152 halfway out from the central axis, $Y_0/R_0 = 0.46$. The polar and longitude angles are 70°
153 and 303°, respectively, indicating that the rope was highly inclined to the MSO X-Y
154 plane and close to the upstream IMF direction.

155 The model fit to the M2 high-field-intensity event at 08:48:30 observed just
156 upstream of the magnetopause is shown in Figure 2b and parameters listed in Table 1
157 (as event 5). Although the best-fit model does not reproduce the extreme peak field
158 intensity, the angular variations in the magnetic field direction are well matched. The fit
159 quality factors are acceptable, with $Q_\chi = 0.140$ and ASF = 0.17. The inferred radius of
160 the flux rope is 0.49 R_M, and the maximum axial magnetic field intensity is 108 nT. The
161 spacecraft closest approach distance to the central axis of the flux rope was again about

162 halfway out from the axis with $Y_0/R_0 = 0.52$. This flux rope had a latitude angle of θ_A =
163 58°, while the longitudinal orientation was sunward at $\phi_A = 355°$. The fit results for the
164 three remaining magnetosheath FTEs are graphed in Figure 3, and their fit parameters
165 are listed in Table 1.

166

167 **4. Summary and Conclusions**

168 The MESSENGER FTEs are significantly longer in duration than the ~ 1-s
169 Mariner 10 FTEs identified and analyzed by *Russell and Walker* [1985]. Only two of
170 the six MESSENGER FTEs are less than 2 s in duration, while the other four have
171 durations of 3.4 to 7.1 s. The reason why the MESSENGER FTEs are larger is unclear,
172 but it may be due to differences in upstream solar wind conditions between the
173 MESSENGER and Mariner 10 flybys. The 32-s interval between the two M2 FTEs is
174 similar to the ~30–40-s period large-amplitude magnetospheric compressional
175 perturbations reported by *Anderson et al,* [2009] and the ~ 30–60-s spacing between
176 the plasmoid and traveling compression regions in the tail found by *Slavin et al.*
177 [2009a]. The comparability of these periods raises the possibility that the formation and
178 tailward motion of FTEs may produce global compressions of the forward
179 magnetosphere and episodes of reconnection in the tail.

180 Our modeling indicates that the MESSENGER FTEs can be represented as quasi-
181 force-free flux ropes. Their diameters and axial magnetic flux contents varied from D =
182 0.15 to 0.98 R_M and $\Phi = 0.001$ to 0.2 MWb. The largest of the FTEs observed by
183 MESSENGER have diameters that exceed by a factor of ~2 the mean thickness of the
184 magnetosheath at the local time when they were observed. However, it must be noted

185 that MESSENGER does not make the high time resolution plasma moment
186 measurements that would be required to infer FTE flattening using GS reconstruction
187 techniques. Given their great relative size, these FTEs could be significantly deformed
188 by their interaction with the magnetosheath and the shape and location of
189 magnetopause and bow shock locally altered. By comparison, the typical FTE observed
190 at the Earth has a diameter of ~ 1 Earth radius (R_E) which is only ~30% of the mean
191 subsolar magnetosheath thickness at Earth. Furthermore, the axial magnetic flux of the
192 largest MESSENGER FTEs approaches that of FTEs observed at Earth [*Zhang et al.*,
193 2008; and references therein]. This result suggests that FTE size may be controlled not
194 by the dimensions of the magnetosphere, but by the plasma kinetic properties of the
195 solar wind or the reconnection process as has been previously suggested [*Kuznetsova*
196 *and Zeleny,* 1986]. The variation in tail lobe magnetic flux from relatively quiescent,
197 northward IMF, to more active, southward IMF intervals at Earth and Mercury are
198 estimated to be ~ 500 to 700 MWb [*Huang et al.,* 2009] and 4 to 6 MWb [*Alexeev et*
199 *al.,* 2009], respectively. Hence, while a large FTE at Earth transports perhaps 0.1% of
200 the quiet time lobe flux, the situation at Mercury is quite different with a large FTE
201 carrying ~ 5% of the total lobe flux. The transfer of this magnetic flux from the
202 dayside to the nightside magnetosphere will contribute an amount, $\Phi/\Delta T$ where $\Delta T \sim$
203 D/400 km/s is the time scale for the flux change to the dawn-to-dusk magnetospheric
204 electric potential. The values range from ~ 1 kV for the smallest to ~ 30 kV for the
205 largest MESSENGER FTEs.
206 The magnetic flux content of the FTEs observed by MESSENGER may also
207 have significant implications for solar wind access to the surface and, therefore, for the

variability in the sputtered component of Mercury's exosphere. For IMF B_X oriented away from the Sun and $B_Z \sim$ -10 nT, i.e., conditions close to those during MESSENGER's second flyby, *Sarantos et al.* [2007] estimated that 12% of the northern hemisphere is magnetically "open" and exposed to the solar wind. Magnetic flux conservation indicates that a 0.2 MWb FTE will expose an additional ~ 10-20% of the surface to solar wind impact. However, this newly open magnetic flux will be concentrated in the cusp regions where most of the solar wind ion precipitation occurs [*Sarantos et al.,* 2007]. For this reason FTEs may produce brief increases in solar wind ion impact with amplitudes of many tens of percent relative to the mean cusp precipitation rate and the rate at which neutrals are sputtered into Mercury's exosphere.

Acknowledgments. Computational assistance and data visualization support provided by J. Feggans are gratefully acknowledged. Conversations with S. Imber and A. Glocer are appreciated. The MESSENGER project is supported by the NASA Discovery Program under contracts NASW-00002 to the Carnegie Institution of Washington and NAS5-97271 to the Johns Hopkins University Applied Physics Laboratory.

References

Alexeev, I. I., *et al.* (2009), Mercury's magnetospheric magnetic field after the first two MESSENGER flybys, *Icarus,* submitted.

229 Anderson, B. J., M. H. Acuña, H. Korth, M. E. Purucker, C. L. Johnson, J. A. Slavin, S.
230 C. Solomon, and R. L. McNutt, Jr. (2008), The structure of Mercury's magnetic
231 field from MESSENGER's first flyby, *Science, 321*, 82–85.
232 Anderson, B. J., *et al.* (2009), The magnetic field of Mercury, *Space Sci. Rev.*, in press.
233 Eriksson, S., et al. (2009), Magnetic island formation between large-scale flow vortices
234 at an undulating postnoon magnetopause for northward interplanetary magnetic
235 field, J. Geophys. Res., 114, A00C17, doi:10.1029/2008JA013505.
236 Fear, R. C., S. E. Milan, A. N. Fazakerley, C. J. Owen, T. Asikainen, M. G. G. T.
237 Taylor, E. A. Lucek, H. Rème, I. Dandouras, and P. W. Daly (2007), Motion of flux
238 transfer events: A test of the Cooling model, *Ann. Geophys.*, *25*, 1669–1690.
239 Huang, C.-S., A. D. DeJong, and X. Cai (2009), Magnetic flux in the magnetotail and
240 polar cap during sawteeth, isolated substorms, and steady magnetospheric
241 convection events, *J. Geophys. Res.*, *114*, A07202, doi:10.1029/2009JA014232.
242 Kuznetsova, M. M., and L. M. Zeleny (1986), , in *Proceedings of the Joint Varenna-*
243 *Abastumani International School and Workshop on Plasma Astrophysics, Sukhumi,*
244 *USSR, 19 to 28 May 1986*, SP-251, European Space Agency, Noordwijk, The
245 Netherlands, pp. 137–146.
246 Lepping, R. P., J. A. Jones, and L. F. Burlaga (1990), Magnetic field structure of
247 interplanetary magnetic clouds at 1 AU, *J. Geophys. Res., 95*, 11,957–11,965.
248 Lepping, R. P., D. B. Berdichevsky, C.-C. Wu, A. Szabo, T. Narock, F. Mariani,
249 A. J. Lazarus, and A. J. Quivers (2006), A summary of WIND magnetic clouds
250 for years 1995-2003: Model-fitted parameters, associated errors and
251 classifications, *Ann. Geophys.*, *24*, 215-245.

252 Lundquist, S. (1950), Magnetohydrostatic fields, *Ark. Fys.*, *2,* 361-372–.

253 Owen, C. J., A. Marchaudon, M. W. Dunlop, A. N. Fazakerley, J.-M. Bosqued, J. P.
254 Dewhurst, R. C. Fear, S. A. Fuselier, A. Balogh, and H. Rèmy (2008), Cluster
255 observations of "crater" flux transfer events in the dayside high-latitude
256 magnetopause, *J. Geophys. Res.*, *113*, A07S04, doi:10.1029/2007JA012701.

257 Russell, C. T., and R.C. Elphic (1978), Initial ISEE magnetometer results:
258 Magnetopause observations, *Space Sci. Res., 22*, 681–715.

259 Russell, C. T., and R. J. Walker (1985), Flux transfer events at Mercury, *J.*
260 *Geophys. Res.*, *90*, 11,067–11,074.

261 Sarantos, M., R. M. Killen, and D. Kim (2007), Predicting the long-term solar wind
262 ion-sputtering source at Mercury, *Planet. Space Sci., 55*,1584–1595.

263 Slavin, J.A., *et al.* (2008), Mercury's magnetosphere after MESSENGER's first flyby,
264 *Science, 321*, 85–89.

265 Slavin, J. A., *et al.* (2009a), MESSENGER observations of magnetic reconnection in
266 Mercury's magnetosphere, *Science, 324,* 606–610.

267 Slavin, J. A., *et al.* (2009b), MESSENGER observations of Mercury's magnetosphere
268 during northward IMF, *Geophys. Res. Lett., 36*, L02101,
269 doi:10.1029/2008GL036158.

270 Trávníček, P. M., D. Schriver, P. Hellinger, D. Herčík, B. J. Anderson, M. Sarantos, J.
271 A. Slavin (2009), Mercury's magnetosphere-solar wind interaction for northward
272 and southward interplanetary magnetic field: Hybrid simulation results, *Icarus*,
273 submitted.

Wang, Y. L., *et al.* (2005), Initial results of high-latitude magnetopause and low-latitude flank flux transfer events from 3 years of Cluster observations, *J. Geophys. Res.*, *110*, A11221, doi:10.1029/2005JA011150.

Zhang, H., K. K. Khurana, M. G. Kivelson, V. Angelopoulos, Z. Y. Pu, Q.-G. Zong, J. Liu, and X.-Z. Zhou (2008), Modeling a force-free flux transfer event probed by multiple THEMIS spacecraft, *J. Geophys. Res.*, *113*, A00C05, doi:10.1029/2008JA013451.

[1]Heliophysics Science Division, NASA Goddard Space Flight Center, Greenbelt, MD 20771, USA

[2]Naval Research Laboratory, Washington, DC 20375

[3]The Johns Hopkins University Applied Physics Laboratory, Laurel, MD 20723, USA

[4]Office of Space Research and Technology, Academy of Athens, Athens 11527. Greece

[5]Laboratory for Solar and Atmospheric Physics, University of Colorado, Bounder, CO 80303, 20771

[6]Solar System Exploration Division, NASA Goddard Space Flight Center, Greenbelt, MD 20771, USA

[7]Institute for Geophysics and Planetary Physics, University of California, Los Angeles, CA 90024

[8]Department of Terrestrial Magnetism, Carnegie Institution of Washington, Washington, DC 20015, USA

[9]Astronomical Institute, Academy of Sciences of the Czech Republic

297 [10]Department of Atmospheric, Oceanic and Space Sciences, University of Michigan,
298 Ann Arbor, MI 48109, USA
299

Table 1. Flux Transfer Event Modeling Results

Event	DOY	Start Time UTC	Duration (s)	Q_χ	ASF	H*	R_0** (R_M)	$\lvert Y_0/R_0 \rvert$	B_0 (nT)	θ_A (°)	ϕ_A (°)	Φ (MWb)
1	014	18:32:24	0.97	0.101	0.12	L	0.078	0.53	20.9	-53.9	254.9	0.0011
2	014	18:34:27	3.42	0.049	0.055	L	0.35	0.69	30.3	5.7	132.3	0.030
3	014	18:36:20	6.00	0.082	0.202	L	0.52	0.46	38.7	69.8	302.9	0.085
4	014	19:16:19	1.37	0.169	0.000	L	0.086	0.00	57.5	12.8	228.9	0.0035
5	280	08:49:25	7.09	0.140	0.169	R	0.49	0.52	108.2	58.0	354.8	0.22

* H is handedness: R for right-handed and L for left-handed.

** $V = 400$ km/s is assumed for all cases except event 5, for which $V = 250$ km/s.

307

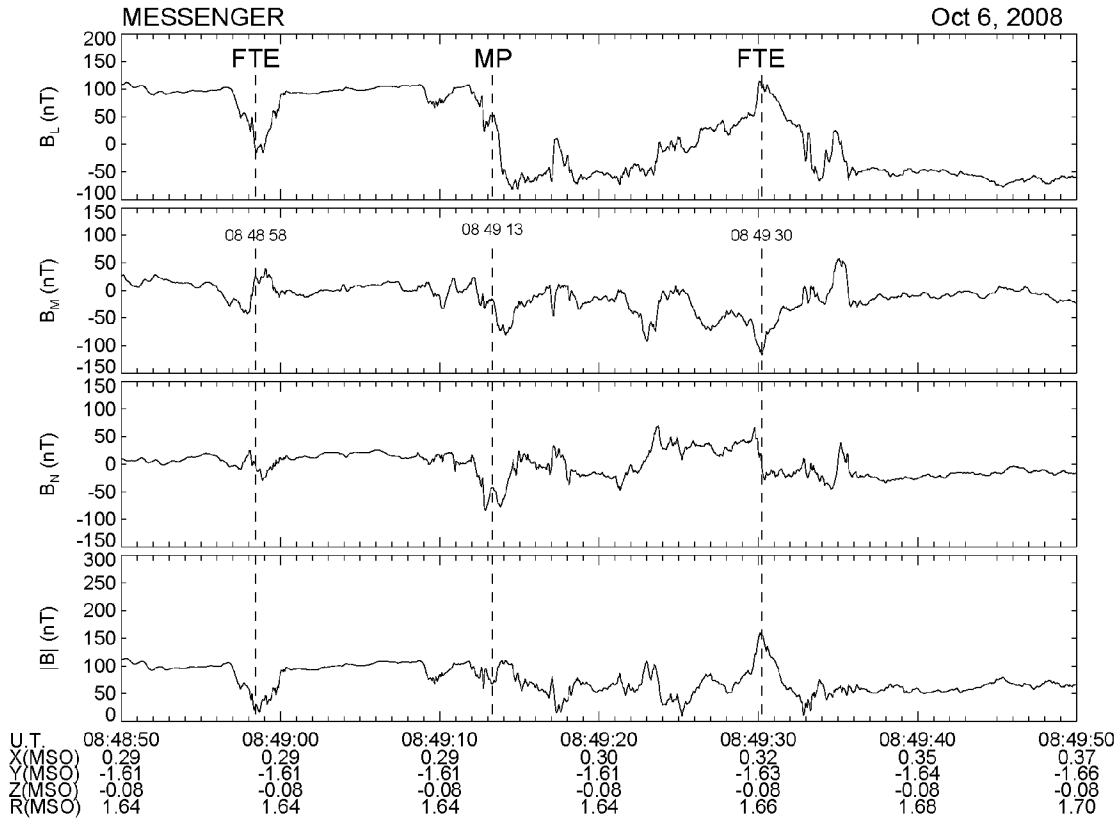

308

309 Figure 1. MESSENGER magnetic field measurements across the M2 dawn

310 magnetopause in boundary normal coordinates.

311

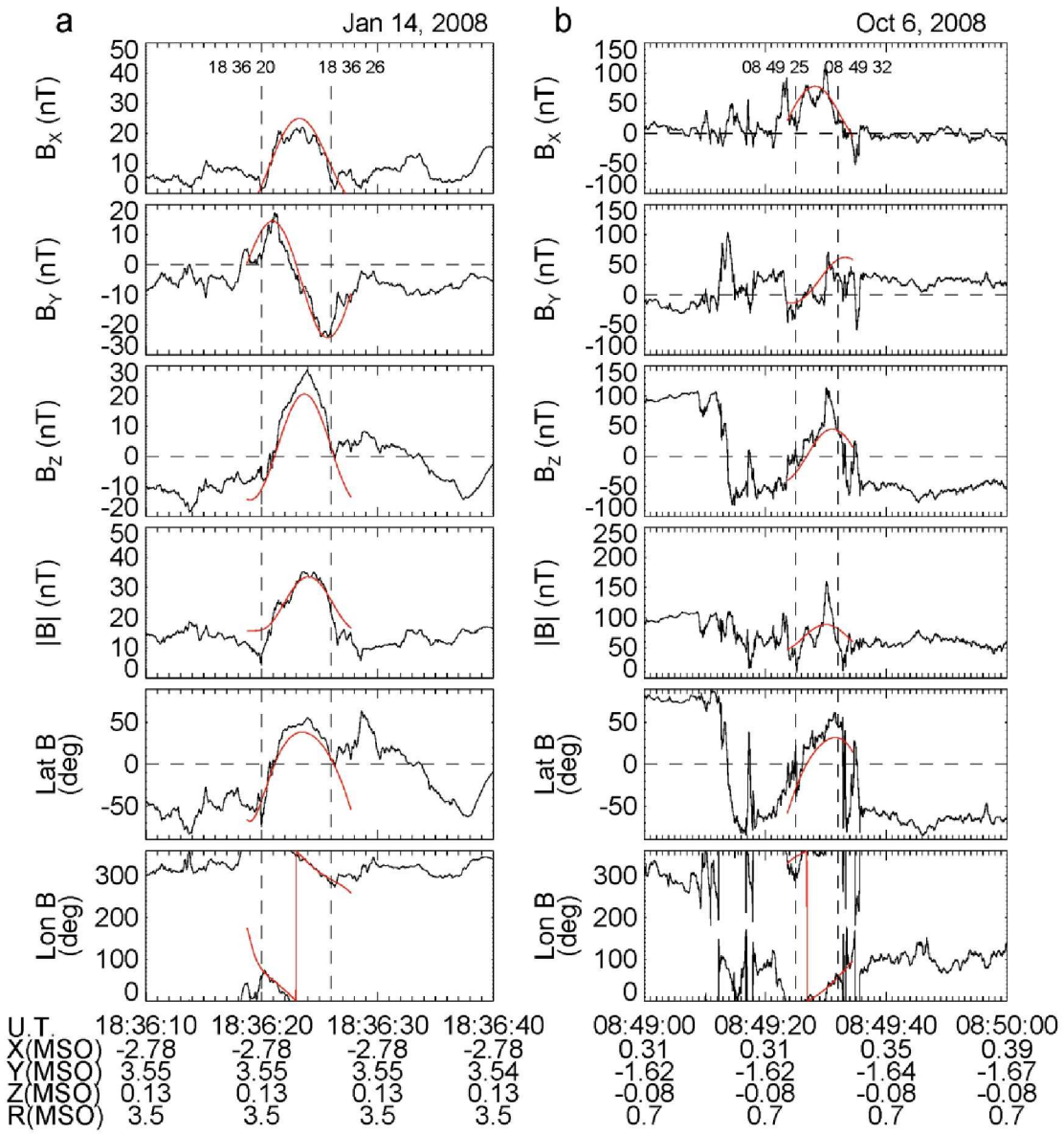

Figure 2. Magnetic field measurements in MSO coordinates for the largest FTEs identified during (a) M1 and (b) M2. Force-free flux rope models fit to these events are shown in red. Dashed vertical lines mark the selected beginning and end of the fitting interval. Due to its location in the magnetosheath sunward of the dawn terminator, a speed of 250 km/s is assumed for the M2 FTE.

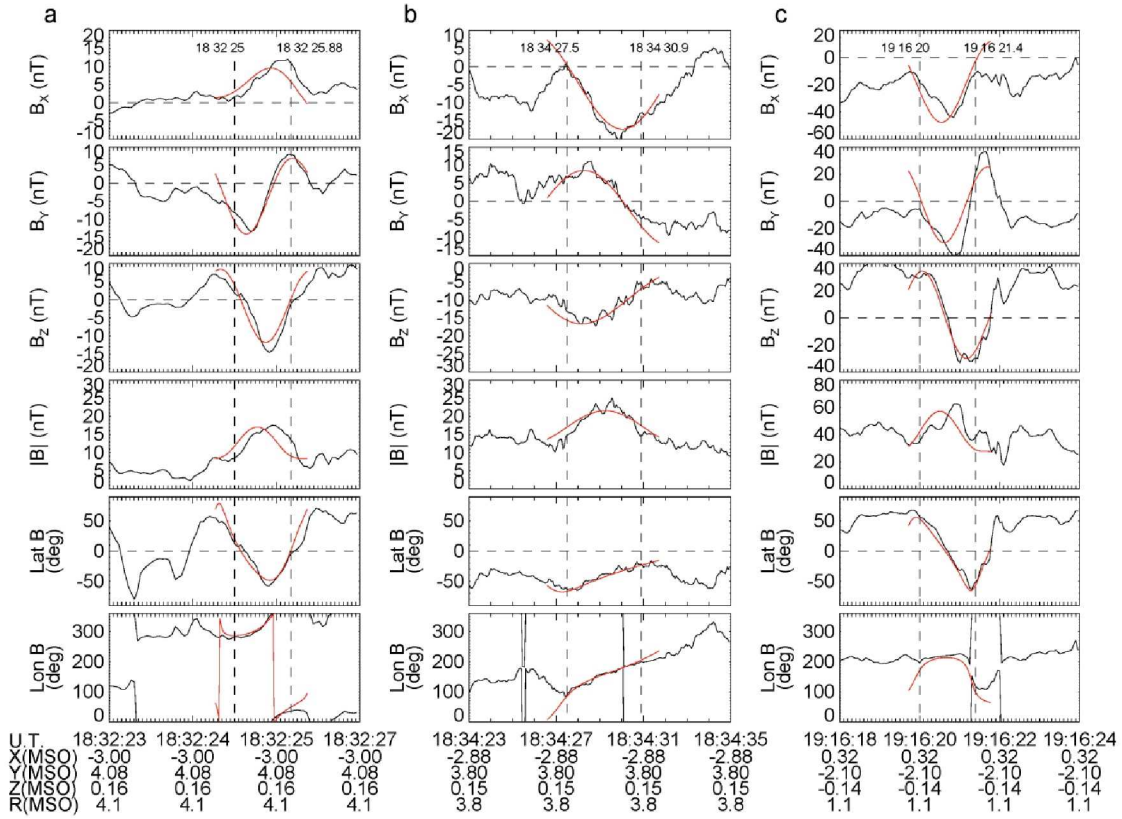

Figure 3. Magnetic field measurements of FTEs observed during M1 with constant-α flux rope models shown in dark red.